Molecular Dynamics Study of Coagulation in Silica-Nanocolloid–Water–NaCl Systems Based on the Atomistic Model

Journal:	*Physical Chemistry Chemical Physics*
Manuscript ID:	CP-ART-07-2014-002984.R1
Article Type:	Paper
Date Submitted by the Author:	03-Sep-2014
Complete List of Authors:	Habasaki, Junko; Tokyo Institute of Technology, Department of Innovative and Engineered Materials Ishikawa, Masamichi; Riken, Research Cluster for Innovation Business Development Office

Molecular Dynamics Study of Coagulation in Silica-Nanocolloid–Water–NaCl Systems Based on the Atomistic Model

Junko Habasaki*† and Masamichi Ishikawa**

*Department of Innovative and Engineered Materials, Interdisciplinary Graduate School of Science and Engineering, Tokyo Institute of Technology, Nagatsuta 4259, Yokohama 226-8502, Japan

** Research Cluster for Innovation Business Development Office, Riken, 2-1 Hirosawa, Wako, Saitama 351-0198, Japan

† To whom correspondence should be addressed.

E-mail: habasaki.j.aa@m.titech.ac.jp

Abstract

In the present work, large scale molecular dynamics (MD) simulations of nanocolloidal silica in aqueous NaCl solutions were performed using a fully atomistic model to study the microscopic structures and dynamics of the systems that lead to aggregation or gelation. Our attention is focused on the self-organizations that occur in the structures of the colloidal silica and water for various concentrations of NaCl. As the salt concentration increased, coagulation developed through the direct bonding of SiO_4 units. The trend was explained by the systematic changes in the pair correlation functions related to the barrier height in the potential of mean force [J. G. Kirkwood, J. Chem. Phys., 1935, **3**, 300].

Network structures of silica were visualised, and their fractal dimensions were examined by computing the running coordination numbers of Si-Si pairs and also by the analysis of two dimensional images. The calculated dimension by the former method was comparable to the experimental observations for the aggregation of silica colloids, and at longer length scales, super-aggregation was evident in the gelation process. The result from the 2D images is found to be insensitive to the differences in the structure. Clear changes in both the structure and mobility of the water were observed as the NaCl concentration increased, suggesting the importance of the solvent structures to these processes, although such a feature is lacking in the conventional models and most simulations of colloids.

I. INTRODUCTION

Colloidal systems play important roles in many fields, including the pharmaceutical and biotechnology fields [1-3], as well as industry and environmental chemistry [4-7]. In practical applications, coagulation using colloidal silica or sodium silicate is a useful technique for extracting heavy metals from water to address the problem of environmental pollution [5]. However, silica scale is also known to cause the plugging of pipelines in geothermal power stations [6] and desalination systems [7]. A thorough understanding of the mechanisms of aggregation and gelation is of fundamental importance to the ability to control these processes.

The DLVO (B. Derjaguin – L. L. E. Verwey and T. Overbeek) theory [8] is frequently used to explain the stability of colloidal systems. Most works of colloidal systems seems to assume interactions similar to those of the DLVO model a priori. However, the true nature of the forces that act amongst colloidal particles is a question of long standing [9-11]. There are some gaps between the simplified model used and experimental observations. For example, many experiments suggest the existence of an attraction term acting within colloids [12-15]; evidence for this phenomenon includes the existence of stable voids [13] and phase separation in charged colloids [14, 15]. It is worth noting that the existence of voids also suggests some contribution of the solvent in the aggregation or gelation process. On the other hand, due to commonly observed fractal structures, physical formation of aggregate is considered to be rather general [16] and more simplified models are also used [17,18], although it is not clear what a coarse-graining level is sufficient for the formation of aggregation or gels.

There are practical reasons to use coarse-grained or simple models from the beginning. Usually, it is difficult to include full structures due to a large size difference of colloids and solvent molecules. Huge resources and time are required for such calculations. Therefore large scale MD simulations including structure of both colloids and solvents are challenging. In the present work, the structural and dynamical properties of silica nanocolloidal systems with water and salt were examined in several concentration regions to learn the contribution of factors, which were not included in the most of previous models,

to the self-organized structural formations. Our attention is focused on the structure of the silica network (composed of SiO_4 units) and its fractal dimension. Changes of structures and dynamics of solvent with the concentration of the salt in these systems are also examined. A large scale (containing 30000~55000 atoms), classical MD simulations using a full atomistic potential model derived from *ab initio* calculations were used for this purpose. It exhibits aggregation and gelation without any prior assumption of the underlying mechanism of these behaviours. Large system sizes were necessary because of the size difference between the colloids and the solvent molecules and to ensure that long length scales could be covered for the characterisation of the gel.
Following characterizations for the self-organized structures starting from the atomic level MD simulation seem to be done for the first time, as far as we know.

The concept of the potential of mean force (PMF), which was introduced by Kirkwood [19], plays an important role in statistical mechanical theories of liquids. Pair-correlation functions g(r) of long ranged structures related it were examined and systematic changes of g(r) corresponds to the barrier heights in PMF were found. They explain the trend of the coagulation instead of the DLVO model.

Network structure was characterized by the fractal dimension analysis both by 2 and 3 dimensional methods. The fractal dimension obtained by these methods is not the same and it causes a question for the universality of the fractal dimension suggested from the 2D images of structures. The fractal structure examined from a microscopic level reveals a formation of the super-aggregates as suggested from the experimental findings [20] and is characterized as a multifractal.

We also report observations concerning the structural and dynamical changes in the water that arise with variations in the salt concentration. Development of the aggregation is clearly accompanied with the slowing down of the solvent dynamics.

Generally, MD model itself is a valid physical model to be examined.
The MD model used here can be a basis to consider the behaviours of the coagulated system and further modifications, even though it was not fully realistic for considering the details such as surface structures.

II. MOLECULAR DYNAMICS SIMULATIONS

Each model of silica, water, water–salt, and salt interactions is based on *ab initio* MO calculations at the appropriate levels. Further details are provided in the Appendix.

The SPC/E model [21] was used for water because its parameters have been well tested (for example, see [22]) and because parameters for interactions with NaCl salt are available. The water model with fixed bonds was treated using the SHAKE algorithm [23] (the tolerance for the convergence of the bond lengths was set to $10^{-5\sim-6}$). For the colloidal silica, the potential model developed by Tsuneyuki *et al.* [24] (the TTAM (Tsuneyuki-Tsukada-Aoki-Matsui) model) was used. This model is known to successfully reproduce many polymorphs of silica; therefore, it can represent many local structures with different Si-O distances and different O-Si-O and Si-O-Si angles.

The MD simulation was first performed in the *NPT* ensemble, and a simulation in the *NVE* ensemble then followed after the equilibration of the system. The DLPOLY4.01 program [25] was used for the MD simulations. The details of the simulations for subsystems and complex systems are as follows.

A Modelling of colloidal systems

An initial colloidal unit composed of SiO_2 was prepared as an isolated partial system. At first, as an initial unit of colloids, a model of colloidal silica consisting of 108 atoms was equilibrated starting from a random configuration in the NVE ensemble at 3000 K with a periodic boundary condition (PBC). The volume was fixed to the value obtained from the NPT ensemble (using a Nosé–Hoover thermostat and a barostat [26]) under atmospheric pressure. Then the system was cooled down gradually (cooling rate was ~1 K/ps) to 2000 K. At this stage, density of the system was found to be 2.4 g cm^{-3}. After equilibration at 2000 K under constant pressure (0.1 MPa), the PBC was removed and condition was changed to NVE [27]. The rounded shaped silica unit was formed within ~2 ns run (2,000,000steps). After that the system was quenched to 300K by scaling of temperature and was equilibrated at the temperature.

For this non-periodic system, the Coulombic force was calculated as a direct sum.

B Construction of the initial configuration of complex system with colloidal units, water and salt

The colloidal unit thus prepared was solvated with SPC/E water, and Na^+ and Cl^- ions were then added. The solvated system containing one colloidal unit was subjected to a PBC. The Coulombic force was treated by a particle-mesh Ewald summation [28] (the tolerance was set to $10^{-4\sim-6}$ [29]) in the system with the PBC.

After equilibration at 300 K in the NPT ensemble, a basic cell was prepared for the MD simulations by creating 64 (4x4x4) repetitions of the solvated unit colloid cell, where the system is locally equilibrated. Six types of systems — I-A, B, and C and II-A, B and C — with PBCs were examined in the present work. The series II systems contain a larger amount of water than those of the I series, and system II-A is a reference system that does not contain a salt.

Descriptions of the systems, including the number of colloidal units and atoms, the number of Na^+-Cl^- pairs, and the concentration of salt in the solution, are provided in Table 1.

C. Further equilibration toward formation of aggregations or gel

Then further runs of self-organization process toward the equilibrium of the whole system were done for these systems. Equilibrations of the large systems usually require long time runs. We used a pre-equilibration at higher temperature than the room temperature to accelerate them. Each system (except I-C) was equilibrated at 400 K until the energy of the system became nearly constant, and the temperature was then decreased to 300 K for the final equilibration. Each time step was set to 1 fs. After the pre-equilibrated for 1~3 ns, further runs have been done with monitoring the structures and energies of the system. When the energies and structures of one 100,000-step run (1 step=1 fs) were essentially maintained in the subsequent 100,000-step run, the system was considered to be sufficiently equilibrated, and the simulations were continued on a longer time scale for statistical treatment of data. After the equilibration of the system, the ensemble was changed to NVE, using the volume obtained from the NPT run. The results for the time range of 400 ps to 2 ns (400,000~2,000,000 steps) at 300 K after the

equilibration run were of primary interest to us. Beginning from the I-B configuration, the temperature was again increased to 400 K to accelerate coagulation; the resulting system is denoted by I-C. We observed the developments of infinitive networks in this system, in which the atoms became immobile. This system is regarded as a gel in the present model. The gel thus obtained was quasi-equilibrated because of the slow dynamics.

The size of the basic cell for the MD simulations, L, of the complex system addressed the present work was 65~90 Å. To examine g(r) at a long length scale, an additional run was performed in each system with a long cut-off length of ~L/2 (for both the short-length-scale force and the real part of the electrostatic force), whereas a cut-off length of 12 Å was used in all other cases. Although we used systems as large as possible within the limitation of calculation resources and times, further check of the finite-size effects will be desired.

D. Structure of a colloidal unit

In Fig. 1 (a), the structure of a colloidal unit is illustrated using a ball-and-stick model. In Fig. 1(b), the same structure is illustrated using a polyhedral (SiO_4 units) model to represent the packing and the connections amongst tetrahedral units. Typically, oxygen atoms serve a bridging function in this structure. On the surface of the unit, 13 non-bridging oxygen atoms are observed (of 72 total oxygen atoms), and there are seven Si atoms coordinated by three bridging oxygen atoms. The former can be regarded as a negative charge centre, whereas the latter acts as a positive charge centre in this model (at least prior to solvation), although the sum of all charges in the unit was set to zero in the present work. There are two polyhedral complexes composed of two SiO_4 units with shared edges. The other SiO_4 units are connected by shared corners.

The colloidal particles used in experiments are typically on the order of nm or μm in size. The system addressed in the present study, with a diameter of ~1.5 nm for each silica cluster unit, might be regarded as a minimum colloid model. In this case, the time separation between the motion of the silica colloid and the water molecules is not significant, and the dynamics of the colloidal particles might be directly affected by the motion of molecules or atoms. Previously, the microscopic structure of nanometre-sized

silica particles has been examined by Uchino *et al.* [30] using infrared and Raman spectra as well as X-ray diffraction analysis. These authors demonstrated that the structure of nanometre-sized particles of fumed silica is not identical to that of the bulk material. In particular, with regard to the size distribution of the silica rings, three- and four-membered rings are more common in fumed silica than in bulk silica glass. In MD simulations of silica at the nanoscale [31,32], clusters can be represented by a shell-like structure, in which the surface is different from the interior of the cluster. In this case, the ‘‘surface shell’’ was shown to have the same thickness and width regardless of the size of the clusters, and the surface width was estimated to be ~2 Å.

E. Size of the colloidal units and related concerns

Harkless *et al.* [33] have examined silica clusters of several sizes based on the TTAM model. For small clusters (~6 SiO_2), the parameters were not necessary sufficient to represent the structure of the cluster [34]. Nevertheless, we can expect the situation to be improved for the colloidal unit (~36 SiO_2) used in the present work as well as for larger aggregates and gels because the TTAM model was optimised for bulk material.

M. Benoit *et al*. [35] have performed a classical simulation of silica glass using the BKS (Beest-Kramer-Santen) model [36]. They also have performed a Car–Parrinello (CP) simulation [37] for the system consisting of 26 SiO_2. For the configurations obtained from classical MD simulations of a system of 216 SiO_2 using the BKS potential, these authors found that the system exhibits remarkable stability in its CP dynamics. They argued that this finding confirms the validity of the BKS potential and also means that the structures of the 26 SiO_2 and 216 SiO_2 systems are comparable. Thus, the colloidal unit used in the present work can be treated by the TTAM model, which is of comparable quality to the BKS model and seems to be sufficient for the purposes of the present work. (The BKS model was determined from *ab initio* MO calculations in a similar manner as the TTAM model and is known to have a slightly improved repulsive term. For our treatment, the functional form of the TTAM model is suitable.)

III. RESULTS AND DISCUSSION

A. Changes in the network structures and the formation of gel

The instantaneous structures of the systems I-A and I-B obtained from the MD simulations after equilibration are depicted in Figs. 2(a) and 2(b), respectively. The spheres representing Si were enlarged to emphasis their positions in the structures. In Fig. 2(a), spherical groups of colloidal units can be observed, but some SiO_4 units are connected by shared edges to form a large network. In both I-A and I-B, the colloidal units form one large aggregate. In the I-B system, which has a greater NaCl content, the connections amongst the units are more developed.

In systems II-A and B, which contain a larger amount of water (by a factor of ~two) than systems I-A and I-B, the network is less developed. In Fig. 3, the silica network of system II-A (without salt) is presented. Some connections amongst colloidal units have developed, but each cluster is separated by water, as is evident from the three-dimensional (3D) views (by rotating the unit, we confirmed the presence of 19 clusters in the basic cell of the simulation), although the colloid appears to form one large aggregate when it is projected onto a plane. Each cluster contains 3.8 colloidal units on average. In Fig. 3(b), a black and white representation of a network projected onto the same plane is depicted. From figures of this type, the fractal dimensions for the medium- and longer-range regions of the 2D projections were obtained (see the caption of the figure). These values are listed in Table 2. The values in the fourth column represent the clustering regions, whereas those in the fifth column represent the connections amongst clusters. The latter value is smaller than former when the clusters are separated by the solvent.

In Figs. 4 the structures of II-C was presented. The largest cluster developed after equilibration. The salt concentration in this system is greater than that in system I-A; however, the network in I-A developed further because of the different ratio of SiO_2 to water.

In system I-C, following a short run (~several hundred ps at 400 K) after the long run at 300 K, we observe a gradual shrinkage (approximately 19% in volume) of the system in *NPT* conditions and the arrest of the dynamics of the system, including the water and the

formation of three-dimensional (infinitive) networks of silica. The networks formed of -Si-O-Si- bonds and the water that was trapped in the network. We regard this 3D percolated structure as gel. In Fig. 5, the structure of the gel is represented by projections onto three perpendicular planes.

The system seems to be more ordered than in the case of typical aggregates, suggesting that the long-range structure of the system may be affected by a periodic boundary. This finding also suggests the existence of long-range cooperative motions.

The dynamics of each constituent of the system, including the solvent, changed considerably with the formation of the gel, as demonstrated later.

B. Fractal dimensions of the network structures

Here a pair correlation function, g(r), for the Si-Si pairs is examined to characterise the networks.

In Fig. 6 (a), the pair correlation functions for the Si-Si pairs of systems I-A, I-C, II-A and II-C are plotted on a linear-log scale, whereas in Fig. 6(b), these correlation functions are plotted on a log-log scale. The series II systems exhibit larger peaks than the series I systems, which indicate more isolated clusters.

I-A and I-C exhibit smaller peak heights than II-A and II-C. For a higher concentration of NaCl, the Si-Si peak heights for the first and several subsequent shells (for dense regions of the networks) decrease, and these dense regions become smaller in both series of systems. A small minimum (deviation from g(r)=1) is observed in the long-length-scale regions (r>12~35 Å) of the dilute systems before g(r)=1 is attained. This trend can be more clearly observed when a logarithmic scale is used for the g(r) value, as shown in Fig. 6 (b).The minimum is located at approximately half of the mean distance between clusters or aggregates when these structures are separated by solvent. The existence of this minimum is consistent with the results of off-lattice diffusion-limited colloid aggregation (DCLA) calculations performed by Hasmy *et al.* [38]. In the pair correlation function, the r=0 position of the function is common to all Si atoms, including those located on the peripheries of clusters. The size of these clusters is several times larger than that of the original SiO_2 colloidal units in our systems. The largest deviation from 1 is observed in the

system without salt (II-A) at approximately r=35 Å. A decrease in the peak heights of g(r) in the short-length-scale region can be observed with increasing NaCl concentration for I-B (not shown); hence, changes occur with coagulation, and therefore, the higher temperature of system I-C has no significant effect on the function.

Thus, in system I-C, the power-law region below r~12 Å represents the spreading of the network of clusters, and the longer-length-scale region represents the development of connections amongst these structures to form a gel.

The concept of potential of mean force (PMF) seems to be well applicable to the colloidal system considered in the present work. To obtain the PMF from simulation runs along reaction coordinates, techniques such as umbrella sampling [39] are required, whereas for equilibrated or nearly equilibrated systems, the PMF, $W_{ij}(r)$, is related to the pair correlation function $g_{ij}(r)$ as follows [40]:

$$W_{ij}(r) = -k_B T \ln g_{ij}(r) \quad (1)$$

Thus, the trend in the PMF can be determined based on the behaviour of g(r), which can be obtained with better statistics using an average for many initial times.

From this functional form, it is clear that the minimum of g(r) corresponds to the barrier for effective repulsive interaction amongst colloidal clusters. As expected, the effective repulsive force is the largest for the system without salt, for which the deepest minimum is observed. In the gel, the length of the power-law region is the shortest amongst all investigated systems, and the minimum is not so clear. The structure of the original colloidal units rapidly decayed and spread to form the gel. The strength of the effective repulsive interaction amongst aggregates is controlled by the salt concentration and the packing density of SiO_2 (SiO_2:water ratio).

The running coordination number $N(r)$ of species j around species i was also obtained from the MD simulations. A power-law region is clearly observed in the log-log plot of N(r), as seen in Fig. 6(c). The function is related to the pair correlation function g(r) as follows [41] when i and j are the same species:

$$N(r) = 4\pi r^2 \sum_n \frac{N_j - 1}{V} g_{ij}(n\Delta r) \quad \text{---- (2)}$$

Here, n is chosen such that nΔr becomes *r*.

The fractal dimensions of the Si aggregates (with and without bonding) for the power-law regions were obtained from the slopes of the log-log plots and are listed in Table 2.

The fractal dimension, d_f, is defined by

$$d_f = \frac{d \log N(r)}{d \log r} \text{ ----- (3)}$$

The corresponding pair correlation function g(r) also exhibits a power-law region with waves,

$$g(r) \sim r^{-A} \text{ ,---(4)}$$

and the dimension d_f is related to A by d_f=*d*-A, where *d* is a dimension of space in this region. Although differences amongst the systems can already be observed in g(r), the value obtained from *N*(*r*) is more accurate and is based on better statistics because of the summation in the definition.

In Fig. 7, the g(r) functions for types of pairs that include Si atoms are presented for systems I-C (gel) and II-A (without salt). As illustrated in Fig. 7(a), the g(r) of the Si-Si pairs and that of the Si-O pairs exhibit opposite oscillations to compensate for the different signs of the charges, as is usually observed in ionic systems [42]. The structures of the Si-Si pairs are formed by both charge-charge and density-density correlations of Si atoms and O atoms. Therefore, both a repulsive force and a long-range Coulombic force contribute to the structural formation of clusters or aggregates. The salt plays a role in severing the network structure or loosely binding different networks together. The contribution of the solvent should also be taken into account. In system II-A, the contribution of the SiO_2 component decreases with increasing *r*, while that of the water component gradually increases. In I-C, the curves of both contributions flatten, indicating a mixing of the solvent component and the silica component in the system.

In Fig. 7 (b) and 7(c), the running coordination numbers *N*(*r*) for every species around Si atoms are presented for I-C (gel) and II-A (without salt), respectively. Water begins to contribute at approximately 2.3 Å in the present model system. As seen in these figures, the

numbers corresponding to HW (hydrogen of water molecule) and OW (oxygen of water molecule) around Si atoms differ notably from system to system. In system I-C, a greater amount of solvent exists near Si than in system II-A. The greater negative slope for Si-Si and Si-O for II-A is balanced with the greater slope for the Si-HW and Si-OW.

The running coordination numbers of the water components rapidly increase with increasing *r*. That is, greater changes in the $N(r)$ slopes are observed for Si-HW and Si-OW than for Si-Si or Si-O in both II-A and I-C. Of course, the contribution of the salt in I-C increases as a function of *r*. The coordination number of Na^+ and/or Cl^- in System I-C (gel) is 20~30 times smaller than that of water in the shorter-*r* region and ~10 times smaller in the longer-*r* region. Therefore a large amount of water comes into a coordination shell of Si or O with addition of the salt and it is related to the change in the slope for Si-Si or Si-O. The water is a counterpart of the silica network to fill the space and is important to structure formation. As demonstrated in the next section, the structure and dynamics of the water change with variations in the salt concentration. Thus, the salt affects not only the interaction amongst colloidal units but also the interaction between the colloid and the water.

In the DLVO model, coagulation caused by the addition of salts might be explained as follows. When a salt is added to a colloidal solution, the width of the charged double layer decreases. If the van der Waals force in the model becomes greater than the electrostatic repulsion, coagulation occurs; that is, the colloid particles are considered to be bound by the attractive van der Waals interaction.

At first glance, the observed situation seems to be similar to the reduction of the zeta potential caused by the salt in the DLVO model, if the assumed potential were to be replaced with the PMF. However, the origin of these forces is not the same as in the DLVO model as shown by the functional form and parameters of the MD model and it was shown that the solvent play roles to form structures. Furthermore, PMF has a collective character. In the present model, the atoms in each silica colloid possess individual charges, while each colloidal unit as a whole is neutral at the beginning of the equilibration process in the simulations. Most of the surface of the colloidal unit in the present work is covered by

bridging oxygen atoms. In spite of these facts, comparable layers of structures found in experiments or in the DLVO model are formed. It can be a basis to examine how it is modified by the surface structures and/or sizes of the colloid and to learn further details of the mechanism.

C. Formation of super-aggregates

The fractal dimension, d_f, of the long-range structure of the aggregates can be determined from the slope of $N(r)$ in the region corresponding to g(r)~1. This region occurs after the power-law region of $g(r)$.

In principal, one can use the region up to ~L/2 for the estimation of the fractal dimension in the MD simulation. The values obtained in this manner are listed in Table 2. Despite the limited length scale addressed by the simulations, the slope could be easily obtained because of the large number of data points.

The numerical error on each fractal dimension reported in Table 2 was estimated to be ± 0.05. In systems I-A, I-B and I-C, we observe fractal dimensions of 2.2~2.4 in the medium-length-scale region. The fractal dimension d_f of I-A is slightly larger than that of I-B or I-C, whereas those for II-A and II-C are comparable. These values reflect a spreading out of the original colloidal units in the solvent but do not directly indicate the development of new connections amongst units.

How do these dimensions correlate with the gelation process? A value of 2.53 is known to be the percolation threshold for a 3D system [43] in the case of random occupation for a three-dimensional cubic lattice; the observed values seem to be slightly smaller than this typical threshold value. On the other hand, in the longer-length-scale region after the minimum (r>12~35 Å), an increase in the fractal dimension is observed for higher NaCl concentrations. The fractal dimension is 2.58 for I-A and ~3.0 for I-B and I-C. Namely, systems I-B (just before gelation) and I-C exhibit similar exponents that indicate three-dimensional connections. The g(r)~1 region is used to investigate the connection of colloidal units or clusters to form gel, as mentioned above. In the case of I-C, the aggregates are thus three-dimensionally connected in the long-length-scale region, whereas

the dimension in the medium-length-scale region is slightly smaller than the percolation threshold, probably because of the existence of solvent-filled voids. The system have different fractal dimensions (exponents) at the two length scales [44].

Fry *et al.* [20] have reported a structural crossover between dilute regions of clusters and cluster-cluster aggregation (super-aggregation) regions based on off-lattice Monte Carlo simulations near gelation, assuming both reaction-limited cluster aggregation and ballistic cluster aggregation. In the dense region, the system possessed a fractal dimension of d_f~2.6 over large length scales, whereas at smaller length scales, the system exhibited the limiting value associated with a dilute state. Sorensen *et al.* [45] have reported structure factors $S(q)$ with large slopes in the small-q regime in the aerogelation of a flame soot aerosol, indicating the existence of the further aggregation of clusters in a dense region. Our results, which were obtained without making any *a priori* assumptions regarding the types of aggregation processes that would occur in the system, are consistent with these previous results.

In systems II-A, II-B and II-C, clusters composed of several colloidal units formed that are separated from other clusters by the solvent. The fractal dimension of the network component was found to be ~2.0. Experimentally, Schaefer et al. [46] have determined the fractal geometry of colloidal aggregates of silica. From the structure factor $S(k)\sim k^{-df}$ obtained from both light and X-ray scattering, they obtained a value of d_f=2.12± 0.05, where a fractal structure of silica was observed in the region of 500~5000 Å. Our values for systems II-B and II-C are comparable to this value. In our systems, the region corresponding to d_f~2 extends to shorter lengths because of the smaller size of the colloidal units.

Weitz *et al.* have identified two distinct regions of aggregates with different fractal dimensions [16] in experiments based on TEM (transmission electron microscopy) images. They observed fractal dimensions of approximately d_f~1.8 for diffusion-limited colloid aggregation and d_f~2.1 for reaction-limited colloid aggregation, and the results were considered to be rather universal. The existence of these two regions can be considered to be analogous to the presence of aggregate and super-aggregate regions. However, neither

our values nor the experimental values obtained by Schafer *et al.* for silica (both for 3D structures) are in agreement with their observations.

Using images like that presented in Fig. 3(b), one can determine the fractal dimensions of 2D projections. For most of our systems, values near d_f~1.8 were obtained (see Table 2), indicating that the 2D values are not sensitive to the differences amongst the systems. To reiterate, the main portion of the plot used for box counting was used to determine the dimension corresponding to clusters or aggregates, and the longer-range region primarily represents the connections amongst these clusters or aggregates. When clusters are connected by a single bond, a fractal dimension of ~1 is observed, whereas when clusters are connected by several Si-O-Si bonds, the fractal dimension is ~2, which is the limiting value for the 2D projection.

One may expect that the projection onto a 2D plane should have an exponent that is comparable to the corresponding 3D value if the fractal dimension is less than 2. However, this was found not to be the case when the fractal dimension was greater than 2 in the 3D observation. Projection onto a two-dimensional plane leads to a considerable degree of overlap of the clusters in the silica network and the voids. The discrepancy between our results and those of Weitz *et al.* may be attributable to the high ($2<d_f<3$) dimensional connection amongst the SiO_4 units in the present system. The fractal dimensions of aggregates or gel may not be clearly obtainable from the analysis of 2D images.

To understand the mechanisms of the formation of aggregates and super-aggregates, further analysis of the bond formation was performed.

D. Number of Si-O bonds and Q_n structures

To understand how the number of connections in the network changes system by system, the number of Si-O bonds in each system was counted using a cut-off length of 2.1 Å. The distribution of Q_n structures (where n is the number of bridging oxygen atoms in the SiO_4 units) was used to characterise each network system. To date, this distribution has been used to characterise glasses and crystals both in experiments [47] and in MD simulations [48]. It has also been used to characterise the surface structure of silicic acid in water using

MD [49]. In that work, it was shown that water acts as catalyst in the polymerisation of silicic acid.

The distributions of Q_n structures determined in the present work are listed in Table 3. The small Q_5 values found for the SiO_5 unit are included. The mean number of bridging oxygens, N_{bo} (for Si-(O)-Si connections), in each system was determined, and these values are also listed in this table. Interestingly, all N_{bo} values are in the range 3.7~3.9, and no remarkable changes amongst the systems are evident. That is, the total number of bonds in each SiO_4 unit remains unchanged during the aggregation and gelation processes, and therefore, the equilibration between bridging and non-bridging oxygen atoms is not affected by the NaCl concentration nor the packing density. This number reasonably explains the observed fractal dimension of ~2 in the clusters: In the first shell of SiO_4 units, a number of units equal to N_{bo} (~3.8) exist, and in the next shell, N^2_{bo} units exist. In the third shell, the number increases to N^3_{bo}. The total number of units present in each shell approximately increases proportional to r^2, where the value of 2 corresponds to the fractal dimension obtained for clusters with bonding.

From these results, it can be concluded that the cluster structure is formed by the reconstruction of networks, that is, both bond breaking within each colloidal unit and the formation of new bonds amongst units. Even in the gel, the local structures are similar to those of the other aggregates. The formation of gels is related to that of structures at longer length scales, as already observed in g(r) and N(r). The coordination number for Si around Si also represents possible connections in the network, as does n in the Q_n structure.

E. Changes in the structure of the water with variations in the NaCl concentration

The pair correlation functions, g(r), for HW-HW, HW-OW and OW-OW pairs are presented in Figs. 8(a), (b) and (c) for systems I-A, I-B and I-C, respectively. The peak at approximately 2.8 Å in the OW-OW function becomes sharper as the NaCl concentration increases, and the shoulder at 3.3 Å becomes clearly visible. The position of the first peak of the OW-OW function shifts slightly towards smaller r with increasing NaCl concentration. Clearer oscillations in the g(r) functions, especially for OW-OW pairs in the

longer-length-scale region, are observed for higher concentrations, indicating the development of more tightly packed clusters of water. The coordination number of OW around OW in the pure SPC/E water is 4.24 at the first minimum (at 3.23 Å), and the location of the second peak is well separated from this feature, whereas the value is 10.3 at the first minimum (at 4.03 Å) after the shoulder for I-C (gel). Therefore, in the gel, the second shell collapsed.

The peak height of the pair correlation function corresponding to OW-HW pairs also increases with increasing NaCl concentration. These trends are consistent with the decrease in the mobility of the water discussed in sections III F and G.

It is interesting to note that the structural change in the water that is observed with variations in the NaCl concentration is comparable to the transition between a high-density liquid (HDL) and a low-density liquid (LDL) that has been observed in several works [50-52] related to polyamorphism [53]. For example, Soper *et al.* [52] have reported the observation of structural changes in water with varying pressure at 268 K through neutron diffraction. In their work, a transition from open, hydrogen-bonded tetrahedral structures to non-tetrahedral O-O-O angles and collapsed second coordination shells was observed with increasing pressure.

In fact, the volume change observed during gelation process (approximately 19%) in this work is reasonable for such a change from an LDL to an HDL, and it seems to be important to an understanding of the relation between the glass-transition and gelation processes. We confirmed that similar structural changes are observed in MD simulations of water-NaCl systems. Details of this study will be reported in a separate paper.

F. Role of NaCl in structural formation and dynamical changes in water

In the present work, equilibration of the system was accelerated by the run at high temperature. As usual, the equilibration of the system in the MD simulations was evaluated in terms of the energy of the system and the behaviour of the structures. However, because gradual changes in the clusters can be observed with small changes in energy, it is not clear how long the time scale must be to be sufficient for the study of the clustering and gelation

processes in the MD simulations. Based on the mobility of each species, one can judge which local structures are equilibrated and which are not. Common MSD behaviours with several distinct stages are observed in many systems [54,55] with slow dynamics. As has been clarified for the motion of ions in lithium silicate glasses [56,57], after a time $t_{dif,}$ the MSD indicates a diffusive regime, in which particles move from original positions to a certain mean neighbouring distance.

From the MSD shown below, the equilibration is judged to be enough for almost systems. For the gel, the system is regarded in a quasi-equilibrated one. In Fig. 9 (a), the MSDs of each species in the quasi-equilibrated state for I-A are presented as a function of time. The MSDs of Si and O are small and less than 3 $Å^2$ within a 1 ns run. In Fig. 9(a), MSD of water in power law region (<70 ps) has a slope less than 1 (0.84), while it becomes proportional to time after 70 ps. The MSD of Na seems to exhibit an increase parallel to the MSD of colloidal silica, whose value is slightly larger. The motion of Cl^- is greater than that of Na^+, and the slope seems to be nearly comparable to that of water. Therefore, the motions of Na^+ and Cl^- are essentially decoupled. For system I-B, as shown in Fig. 9(b), the silica component is immobile and the slopes of the MSDs of Na^+, Cl^- and water also decrease. The motions of Na^+ and Cl^- are similar to each other (and coupled). The higher concentration of NaCl seems to make the water more rigid (and tightly packed) because of the strong interaction amongst the salts. The role of Cl^- is non-negligible in this case. For example, near Cl^- ions, the H atoms of water molecules tend to gather, thereby affecting the structure of the water and the connections of Na^+ and Cl^-.

G. Change in dynamics with gelation

The MSDs of atoms and ions for system I-C are presented in Fig. 9(c). The slope in the power law region in Fig. 9(c) for water is 0.53 (the exponent smaller than 1 means a large tendency of back correlated motion) and slope becomes ~0 after 30 ps. The MSD curve for each type of particle exhibits a plateau near the region of 100 ps after the start of observation, and we conclude that gelation occurred at this time, because it accompanied with formation of infinitive network shown in Fig.5. Local motions were still observed

there. This structure was not stable, and after some time (~ns), the system returned to a more mobile state. Both bond breaking and bond formation occur in this system, and therefore, the change is naturally reversible before the number of bonds formed amongst the clusters reaches a certain value.
The arrest of motion of solvent in the system is accompanied with the formation of gel networks as shown in Fig. 5, but is not necessarily the result of it. Slowing down of the dynamics have already been observed before the formation of gel for all species. Changes in the solvent structure and the reduction of mobility accompany both the aggregation and gelation processes.

Both fast and slow particles are found in each case. Heterogeneity of the dynamics (and mixing of these motion occurring in a longer time scales) are commonly observed for ionics in the ionically conducting glasses [56,58,59], ionic liquids [60,61] and glass forming liquids[58, 62-64] near the glass transition regimes, water [65], biomaterials[66] and colloids[67,68]. Thus the MSD is determined by a mean behaviour of heterogeneous dynamics [56, 69]. Further details of the dynamical heterogeneity will be reported in a separate paper.

Even in the flat region of the MSD in Fig. 9(c), system still have local mobility. Examples of individual particle motions observed in system I-C are shown in Fig. 10. In the upper panel, the motions of arbitrary chosen four oxygen atoms in the silica part and those in water are shown. Three OW atoms are more mobile than other ones. In the lower panel of Fig. 10, the motions of arbitrary chosen eight Si particles are shown. The motions are localized ones with some heterogeneity.

H. **Other Approaches**

Here, we briefly discuss some other models of colloids. For typical colloidal particles, which are generally larger than the solvent molecules, the details of the structures of the solvents and colloids tend to be neglected. Thus, one typical approach to the study of colloidal systems is based on the mean-field approach, in which the solution is treated as a

homogeneous medium and the interactions amongst colloidal units are the primary focus of the model. To improve the modelling of colloidal systems, many methods have been introduced thus far. For example, Tanaka and Araki have introduced the Fluid Particle Dynamics method [70], in which the electro-hydrodynamic interactions are properly incorporated.

Further examination of the roles of the pH value and the surface of the colloid will also be important for understanding the behaviours of colloids, as the properties of the colloids depend on these factors [71].

Monte Carlo (MC) simulations are beneficial to the study of the aggregation process. Usually, the sticking probability, P_{ij}, seems to be assumed *a priori*, and the results of such studies are therefore model dependent. Using off-site Monte-Carlo simulations, Kim *et al.* [17] have accounted for the surface charges of the colloids in their examination of the effects of pH on the fractal structures of aggregates. In their work, the DLVO theory is used to provide the relation between the experimental process parameters and the P_{ij} value. It will also be useful to apply a full atomistic model to the evaluation of such scenarios because the results of such models do not depend on any assumption of the stacking probability.

Experimentally, it is known that silica surfaces in colloidal systems exhibit a rich variety of behaviours by virtue of the existence of siloxane or silanol, depending on the conditions of preparation and the pH [72]. Surface modifications also affect the properties of colloids and may play important roles under some circumstances.

Thus far, several types of parameters for expressing the potential between the silica surface and the water [72,73] have been investigated. Hassanali and Singer [73] have proposed a set of parameters to describe the potential of a hydroxylated silica surface (based on the BKS model and SPC water) for SiO_2–water interactions. Reactive force fields, such as ReaxFF [74], have been used in several related works [74-78]. Such approaches will be useful in the investigation of the details of reactions on the surfaces of colloids or gels. In these works, assumed initial structures are used. The *ab initio* MD (the Car–Parrinello (CP) method [29]) will be a useful and promising approach to considering the

detailed properties of colloidal surfaces, although this approach is not necessarily suitable for the examination of slow processes such as aggregation and gelation. Extensive calculation resources and long times are required to probe long times and large scales because the dynamics of the gelation process are slow, similar to the glass-transition problem. Even for work based on *ab initio* MD, the time-consuming equilibration of large systems will be necessary. The equilibrated and quasi-equilibrated configurations obtained in our simulations can be used as the initial configurations for such efforts.

Missana and Adell [4] have reported large uncertainties in stability predictions obtained using the DLVO theory; namely, differences in the Hamaker constant or the surface potential can lead quite different predictions. In future work, direct comparisons between the results obtained using MD and those obtained using the DLVO model will be of interest to resolve such difficulties. Other characteristics of colloidal systems that are beyond the capability of the DLVO model have been noted by several authors. These include the importance of attraction caused by depletion forces [79].

These approaches including ours seem to be complementary to understand many kinds of features in the science of colloidal and related systems and coagulation processes.

IV. CONCLUDING REMARKS

In MD or MC simulations of colloidal systems, the colloids and solvents tend to be represented by simple models that lack structural details. For bridging the gap between microscopic and macroscopic descriptions, approaches with different coarse-grained levels might be necessary, especially for nanocolloids. In this paper, we presented the results of full atomistic MD simulations of complex systems of colloidal silica and water as well as the dynamics of these systems with variations in the concentration of salt and/or the packing density of the colloids. Large system sizes allow us to examine the long ranged structures starting from the atomistic simulations. The self-organization of clusters, aggregates and the gel was observed in the simulation. Changes in both the structures and the dynamics of the solvent were observed. It was found that the solvent dynamics play a role in the coagulation process and that a description of the water structure, including the

positions of anions, is necessary, although such factors have tended to be neglected in some previous models.

The power-law regime of the slope of the $g(r)$ or $N(r)$ function of Si-Si pairs is associated with the spreading of the aggregate, whereas that in the longer-length-scale region is associated with the formation of gel with further aggregation. The existence of "super-aggregates" in the gelation process was confirmed in this simulation without assuming the mechanism of the formation. It is well known that the properties of confined water are different from those of bulk water [80]. The findings of the present work explain both the formation of silica gel and properties of confined water.

The following are points to be considered regarding the aggregation and gelation processes.

1. The Si-Si correlation function exhibits a power-law region, and layered structures of colloids (formed through both density-density correlation and charge-charge correlation) are observed. These structures of clusters or aggregates are separated by solvent-rich regions, where the potential of mean force (PMF) exhibits an effective barrier. The barrier height changes with variations in the NaCl concentration and the silica content. In the gel, the power-law region becomes shorter with the addition of NaCl, and its height becomes smaller. These aggregates can undergo further aggregation with a higher dimensionality of $d_f > 2.5$. This behaviour exhibits some similarity to that of the DLVO model; however, the origin of the force and the details of the structures are not the same.
2. The solvent is incorporated into the fractal structure of the system, and the role of the solvent should be taken into account in the aggregation and gelation processes.
3. The addition of NaCl causes changes in the structure and dynamics of the solvent, and the aggregation process is affected by these changes. NaCl not only causes changes near the surface of the colloid but also causes structural changes in the water. This phenomenon may be related to a transition of the water between an HDL state and an LDL state, although further examination for different concentration region and/or other systems is necessary.

Acknowledgements

This research by Junko Habasaki was partly supported by the Ministry of Education, Science, Sports and Culture, Japan, through a Grant-in-Aid for Scientific Research, 23540439, 2011-2014. A part of this research was performed using machine time on Tsubame 2.0 or 2.5 at the Global Scientific Information and Computing Center of the Tokyo Institute of Technology as a Research Project of HPCI systems (Project ID hp120057.).

APPENDIX

A. Potential Parameters

The availability of reliable potential parameters and their consistency (including the consistency of functional forms) in complicated systems are problematic, although many efforts to derive such parameters are underway. In the present work, potential parameters were obtained from the literature to maintain consistency of quality and combinations as much as possible, although further improvement of these parameters might be necessary, depending on the purpose for which they are used. The parameters used in the present work are summarised in Table 4. Coulombic term was used for all combinations of atoms. There are 6 atomic species in the system (Si, O, Na, Cl, OW, HW, where OW and HW represent oxygen and hydrogen, respectively, in water), even if the individual status of each atom is neglected, and therefore, the possible combinations of atoms number at least 21. (Some repulsive interactions (such as those for Si-Na and Si-Cl pairs) can be excluded from further analysis because direct contact between such pairs is nearly impossible.)

Here, we briefly explain the parameters used in the present work.

Tsuneyuki *et al.* [24] first developed potential parameters for silica (TTAM) based on *ab initio* MO calculations at the HF level. Several such sets of parameters can be obtained, by

virtue of the non-linearity of the functional form; the set that represents bulk properties was chosen because the distribution of charges in a small cluster is not the same as that in the bulk. Later, the BKS potential [33] was derived similar manner as the TTAM parameters, and the repulsive parameters for O-O pairs were improved. Further developments of the potential parameters are still in progress [81,82], indicating the difficulty of deriving the exact potential parameters of silica.

In the present work, the TTAM model was used to model a silica colloid, in which the charges for Si and O were set to +2.4 and -1.2, as in the bulk model. The potential function of the TTAM model consists of a Coulombic term, a Gilbert–Ida-type [83] and an r^{-6} term (for the correction of the softness of the oxygen atom.)

$$\phi_{ij} = \frac{z_i z_j e^2}{r} + f_0(b_i + b_j)\exp(\frac{a_i + a_j - r}{b_i + b_j}) - c_i c_j r^{-6} \quad \text{(a1)}$$

The first term on the right-hand side represents the Coulombic interaction. The value of r represents the distance between atoms, and a_i and b_i are the effective radius and the softness parameter, respectively, of atom i with a constant f_0.(=1 kcal mol^{-1}, Here we keep the unit of original paper.) The r^{-6} term in the TTAM type potential is a correction term of the softness of the oxygen.

The repulsive part of the function can be transformed into a Born–Meyer–Huggins (BMH)-type form. $\phi_{ij} = A\exp(B(\sigma - r_{ij}))$ ---------- (a2)

The use of the TTAM model with a Gilbert–Ida-type function offers certain advantages, as listed below.

1. The parameters are additive, not only for pairs but also for atomic species. Therefore, the transferability of the parameters is good.
2. A system with a glass plate can be treated with consistency because we have developed the corresponding potential parameters for alkali silicates [84], where the silica components of the parameters are taken from the TTAM parameters. This feature is important for the study of colloidal systems because recent experimental measurements have revealed that a strong long-range attraction is at work between colloidal spheres confined by charged glass walls [9], although no such attraction has been observed in

analogous measurements in unconfined systems.

3. The functional form is simple and uses a small number of parameters.
4. This functional form or some modification thereof can be used in many types of MD programs.

During the aggregation and gelation processes investigated in the present work, the reconstruction of Si-O bonds was observed.

In the model, the charge-redistribution effect caused by the lengthening of such bonds or changing angles was included in the parameters that represented the total potential surface, because in the MO calculations of the silica cluster used for modelling the Si-O distance and the bond angles were allowed to vary, and the charge distribution follows from these changes. Namely, the charges were fixed only in the fitted parameters, and hence, the TTAM potential could be used to represent bond breaking and bond formation.

The Lennard-Jones part of the SPC/E model is given by the following functional form.

$$\phi_{ij} = 4\varepsilon[(\frac{\sigma_{ij}}{r_{ij}})^{12} - (\frac{\sigma_{ij}}{r_{ij}})^{6}] \text{ --- (a3)}$$

For the interactions between water and silica, parameters were estimated using eq. (a1) after the procedure mentioned below. The parameters of water associated with the LJ form (a3) were transformed into the corresponding parameters for a Gilbert–Ida-type potential by imposing the requirement that the two functions have the same energy-minimum separation and depth and the same behaviour in the large-*r* region (see ref. 85 for the detailed procedure). Thus parameters of the OW-OW interaction for eq. (a1) were determined. Then, they are changed to those for (a2) form. Charge for each OW and HW was kept unchanged.

The interaction between silica and Na^+ or Cl^- was obtained from the CLAYFF Force Field [86]. Here, the potential functions for the repulsive part are given in the following form:

$$\phi_{ij} = D_{ij}[(\frac{R_{ij}}{r_{ij}})^{12} - 2(\frac{R_{ij}}{r_{ij}})^{6}] \text{ -- (a4)}$$

, where the combination rule applied can be represented as follows:

$$R_{ij} = \frac{1}{2}(R_i + R_j) \text{ and } D_{ij} = \sqrt{D_i D_j} \quad \text{-- (a5)}$$

For the model of NaCl in SPC/E water, the interactions were adopted from a study by Joung and Cheatham [87]. These parameters can successfully reproduce both the binding energies of ions to water and the radii of the hydration shells.

Both models in Ref. 86 and 87 use a formal charge for Na^+ and Cl^-. Even under the assumption of fixed charges for the ions, the silica-salt or water–salt interactions are based on MO calculations or the free-energy surface, and the influence of the fixed charge seems to be compensated by other terms, at least near the equilibrated positions. Therefore, the influence of fixing the charges is minor (although it will be relevant for a long-range force or potential).

Table 1 Characteristics of the systems examined in the present work

	Number of colloidal silica units Each unit contains 36 SiO_2 (108 atoms).	Number of Na^+-Cl^- pairs	Number of water molecules	Concentration of NaCl in water (mol%)	Total number of atoms	Temperature (K)
System I-A	64 (6912 atoms)	128	8192	1.56	31744	300
System I-B	64	320	8192	3.90	32128	300
System I-C	64	320	8192	3.90	32128	400
System II-A	64	0	15872	0	54528	300
System II-B	64	160	15872	1.01	54848	300
System II-C	64	320	15872	2.02	55168	300

Table 2 Fractal dimensions of the colloidal systems

	Fractal dimension d_f			
	From $N(r)_{Si\text{-}Si}$. The typical error was estimated to be 0.05.		From projection of the network onto the 2D plane. The typical error was estimated to be 0.05.	
	Region corresponding to the power-law region of g(r)	g(r)~1 region	Region corresponding to clusters or aggregates	Region corresponding to connections amongst aggregates
System I-A	2.40 2.24 2.83	2.58 (Si-Si) 2.55 (O-O) 2.93 (OW-OW)	1.83	2.00
System I-B	2.23 2.41 2.78	3.07 3.09 (O-O) 3.01 (OW-OW)	1.79	1.17
System I-C (gel)	2.25	3.01	1.80	1.43 (mean value of three directions)
System II-A	2.14	2.10	1.80	1.17
System II-B	1.99	2.34	1.78	2.00
System II-C	2.12	2.40	1.81	1.17

Table 3 Distribution of Q_n structures and mean number of bridging oxygens in the systems examined.

System Status / Species	Solvated-unit	System I-A	System I-B	System I-C		System II-A	System II-B	System II-C
		Aggregate	Aggregate	Aggregate	Gel (Infinitive network)	Small Clusters	Small Clusters and Aggregates	Aggregate
Q1	-	-	0.24	-	-	-		-
Q2	3.18	-	3.17	1.06	1.14	0.32	0.37	-
Q3	18.94	15.58	25.98	21.17	21.93	15.63	13.74	13.81
Q4	75.76	78.64	68.84	76.98	75.19	79.76	80.44	80.55
Q5	0	5.62	1.77	0.79	1.74	4.29	5.45	5.58
Mean number of bridging oxygens	3.7	3.9	3.7	3.8	3.8	3.9	3.9	3.9

Table 4. Potential parameters* used in the present work

Atom pair	Functional Type of the repulsive part				c_ic_j(=C) in eq. (a1)	Reference
	Units	A (kcal/mol)	B ($Å^{-1}$)	σ (Å)	(kcal/mol $Å^6$)	
Si-Si	BMH	0.0657	15.2207	1.7376	0	23
O-O	BMH	0.3513	2.846408	4.0948	4951.937	23
Si-O	BMH	0.2085	4.795933	2.9162	1631.177	23
Si-OW	BMH	0.180922	5.527244	2.54965		a)
O-OW	BMH	0.313722	3.187535	3.72835		a)
		ε (kcal/mol)	σ (Å)			
Si-Na	LJ	0.000489	3.1721			86
Si-Cl	LJ	0.000429	4.3226			86
O-Na	LJ	0.1301	2.6378			86
O-Cl	LJ	0.124722	4.246			86
Na-Na	LJ	0.087439	2.439281			86
Na-Cl	LJ	0.055786	3.458469			86
Cl-Cl	LJ	0.035591	4.47657			86
OW-OW	LJ	0.155	3.166			21
Na-OW	LJ	0.115285	2.794991			87
Na-HW	LJ	0.063421	1.419641			87
Cl-OW	LJ	0.073552	3.814179			87
Cl-HW	LJ	0.040462	2.438829			87

a) Potential parameters for silica–water interactions are obtained by eq. (a1) after changing the form of the potential [85] to the Gilbert–Ida type. Then the form was changed to eq, (a2).

b) Potential parameters for water are taken from ref. 21.

* Coulombic terms are also used for all combinations, where the charges found in the references are kept unchanged. One may prefer the SI units for the parameters. However, the units (kcal/mol, ---) were used for convenience to reduce the necessary number of unit conversions. We maintain the number of digits presented in each value here, although the number of significant digits may be smaller.

REFERENCES and NOTES

1 G. Cevc, Advanced Drug Delivery Reviews, **56**, 675 (2004).

2 K. Kataoka, A. Harada, Y. Nagasaki, Advanced Drug Delivery Reviews, **64**, 37(2012).

3 T. K. Jain , I. Roy , T. K. De , and A. Maitra , J. Am. Chem. Soc., **120**, 11092(1998).

4 T. Missana and A. Adell, J. Colloid and Interface Sci., **230**, 150 (2000).

5 K. Subramaniam, S. Yiacoumi, C. Tsouris, Colloids and Surfaces A: Physicochemical and Engineering Aspects, **177**, 133(2000).

6 R. W. Henley, Geothermics,**12**, 307 (1983); H. P. Rothbaum, B. H. Anderton, R. F. Harrison, A.G. Rohde and A. Slatter, Geothermics, **8**,1(1979).

7. K. D. Demadis, Desalination Research Progress, edited by D. J. Delgado and P. Moreno, p. 249, Chapter VI , Nova Science Publishers Inc.,2008.

8. B. Derjaguin, L. Landau, "Theory of the stability of strongly charged lyophobic sols and of the adhesion of strongly charged particles in solutions of electrolytes", Acta Physico Chemica *URSS*,**14**: 633 (1941); E. J. W. Verwey, J. Th. G. Overbeek, Theory of the stability of lyophobic colloids, Amsterdam: Elsevier,1948.

9. N. Ise and H. Matsuoka, Macromolecules, **27**, 5218(1994).

10. J. C. Croker and D. G. Grier, *Phys. Rev. Lett.,***77**, 1897 (1996); M. Ishikawa, S. Ito, R. Kitano, S. Miyoshi and J. Habasaki, to be published.

11. S. H. Behren, D. I. Christl R. Emmerzael , P. Schurtenberger , and M. Borkovec, Langmuir, **16**, 2566 (2000).
12. J. C. Crocker and D. G. Grier, Phys. Rev. Lett., **77**, 1897 (1996).
13. H.Yoshida , N. Ise and T. Hashimoto, J. Chem. Phys., **103**, 10146 (1995).
14. B. V. R. Tata, R. Rajalakshmi and A. K. Arora, Phys. Rev. Lett., **69**, 3778 (1992).
15. S. K, Lai, W. P, Peng, G. F. Wang, Phys. Rev. E**63**, 041511 (2001).
16. D. A. Weitz, J. S. Huang , M. Y. Lin and J. Sung, Phys. Rev. Lett., **54**, 1416(1985); M. Y. Lin, H. M. Lindsay, D. A. Weitz, R. C. Ball, R. Klein and P. Meakin, Nature, **339**, 360 (1989).
17. S. Kim, K-S. Lee, M. R. Zachariah and D. Lee, J. Colloid and Interface Sci., **344**, 353 (2010).
18. K. G. Soga, J. R. Melrose, and R. C. Ball, J. Chem. Phys., 108, 6026(1998); 110, 2280(1999).
19. J. G. Kirkwood, J. Chem. Phys., **3**, 300(1935).
20. D. Fry, A. Chakrabatti, W. Kim and C. M. Sorensen, Phys. Rev. E69, 061401(2004).
21. H. J. C. Berendsen, J. R. Grigera and T. P. Straatsma, J. Phys. Chem., **91**, 6269(1987).
22. P. Mark and L. Nilsson, J. Phys. Chem. A,**105**, 9954 (2001).
23 SHAKE
24. S. Tsuneyuki, M. Tsukada, H. Aoki and Y. Matsui, Phys. Rev. Lett., 61, 869(1988).
25. I. T. Todorov, W. Smith, K. Trachenko and M. T. Dove, J. Mater. Chem., **16**, 1611 (2006).
26. S. Nosé, J. Chem. Phys., **81**, 511 (1984); W. G. Hoover, Phys. Rev. A, **31,** 1695(1985).

27. During the run in NVE condition, mean temperature becomes 2800 K. The temperature is higher than the glass transition temperature, T_g. Aggregation does not depend on T_g directly, because the Si-O interaction related to aggregation is one modified by water and salt.

28. T. Darden, L. Perera, L. Li and L. Pedersen L., Structure, **7**, R55 (1999).

29. Error of the Ewald summation [P. Ewald, Ann. Phys. 64, 253(1921).] depends on the choice of the cut-off length $L_{cut,}$ parameter α and the maximum numbers of wave vectors in the reciprocal space. The tolerance of the Ewald summation is considered with respect to the ideal situation without an error. Practically, the ideal value can be determined with a large $L_{cut,}$ a large number of wave vectors and optimized parameter α, using a curve for the summation plotted against the parameter.

30. T. Uchino, A. Aboshi,1 S. Kohara, Y. Ohishi, M. Sakashita, and K. Aoki, Phys. Rev. B **69**, 155409 (2004).

31. A. Roder, W. Kob, and K. Binder, J. Chem. Phys., **114**, 7602(2001).

32. I. V. Schweigert, K. E. J. Lehtinen, M. J. Carrier, and M. R. Zachariah, Phys. Rev. B **65**, 235410(2001).

33. J. A. W. Harkless, D. K. Stillinger, F. H. Stillinger, J. Phys. Chem., **100**, 1098(1996).

34. S. K. Nayak, B. K. Rao, S. N. Khanna, and P. Jena, J. Chem. Phys.,**109**, 1245 (1998).

35. M. Benoit, S. Ispas, P. Jund and R. Jullien, Eur. Phys. J. B, **13**, 631(2000).

36. B. W. H. van Beest, G. J. Kramer, R. A. van Santen, Phys. Rev. Lett., 1990, **64**, 1955(1990).

37. R. Car, M. Parrinello, Phys. Rev. Lett., **55**, 2471(1985).

38. A. Hasmy, E. Anglaret, M. Foret, J. Pelous and R. Jullien, Phys. Rev. B., **50**, 6006(1994).

39. G. M. Torrie and J. P. Valleau, Chem. Phys, Lett., 1974, **28,** 578 ; D. Trzensniak, Chem. Phys. Chem., **8**, 162(2007).

40. D. Chandler, Introduction to Modern Statistical Mechanics, Oxford University Press, New York, 1987; J. P. Hansen and I. R. MacDonald, Theory of Simple Liquids, 2nd ed., Academic Press, London, 1990; C.G. Gray and K. E. Gubbins, Theory of Molecular Fluids, Vol. 1, Clarendon Press, Oxford, 1984.

41. B. Mandelbrot, Science,155, 636(1967).

42. P. Keblinski, J. Eggebrecht, D. Wolf and S. R. Phillpot, *J. Chem. Phys.*, **113**, 282(2000); J. Habasaki, K.L. Ngai, *J. of Non-Cryst. Solids*, **357**, 446(2011).

43. D. Stauffer, “Introduction to Percolation Theory” Taylor & Francis, London and Philadelphia 1985, and references therein.

44. T. C. Halsy, M. H. Jensen, L. P. Kandanoff, I. Procaccia and B. I. Shraiman, Phys. Rev. A., **33,** 1141(1986).

45. C. M. Sorensen, W. B. Hageman, T. J. Rush, H. Huang and C. Oh, Phys. Rev. Lett., **80,** 1782(1998).

46. D. W. Schaefer and J. E. Martin, P. Wiltzius and D. S. Cannell, Phys. Rev. Lett., **52**, 2371(1984).

47. Bruckner, H.-U. Chun and H. Goretzki, Glastechn. Ber., **51**, 1(1978);
R. Dupree, D. Holland and M.G. Mortzuka, J. Non-Cryst. Solids, **116**, 148(1990).
; J. Du, A.N. Cormack, Journal of Non-Crystalline Solids, **349**, 66(2004).
;C. M. Schramm, B. H. W. *S.* de Jong, and V. E. Parzialet, *J. Am. Chem. Soc.*, **106**, 4397(1984);H. Maekawa, T. Maekawa, K. Kawamura and T. Yokokawa, J. Non-Cryst. Solids, **127**, 53(1991).

48. U. Voigt, H. Lammert, H. Eckert, and A. Heuer, Phys. Rev. B, **72**, 064207(2005).
;J. Du and R. L. Corrales, Phys. Rev. B. ,**72**, 092201(2005).
; J. Du and L. R. Corrales, J. Chem. Phys., **125**, 114702(2006).
; J. Habasaki and K. L. Ngai, J. Chem. Phys., **139**, 064503(2013).

49. N. Z. Rao and L. D. Gelb, J. Phys. Chem. B, **108**, 12418(2004).

50. P. H. Poole, F. Sciortino, U. Essmann, H. E. Stanley, Nature, **360**, 324(1992).

51. D. Liu, Y. Zhang, C. C. Chen, C. Y. Mou, P. H. Poole, S. H. Chen, Proc. Natl. Acad. Sci., **104**, 9570(2007).

52. A. K. Soper and M. A. Ricci, Phys. Rev. Lett., **84**, 2881(2000).

53. O. Mishima, L. D. Calvert, E. Whalley, Nature, **314**, 76(1985).

54. K. L. Ngai, J. Habasaki, Y. Hiwatari and C. Leon, *J. Phys. C: Condensed Matter*, **15**, S1607(2003).

55. K. L. Ngai, J. Habasaki, C. Leon and A. Rivera: *Z. Phys, Chem. ,***219,** 47(2004).

56. J. Habasaki , K. L. Ngai, and Y. Hiwatari, *Phys. Rev.* **E 66**, 021205(2002).

57. J. Habasaki, K. L. Ngai, and Y. Hiwatari, *J. Chem. Phys.*,**120**, 8195(2004).

58 K. L. Ngai, J. Habasaki, C. Leon and A. Rivera: *Z. Phys, Chem.,* **219,** 47-70 (2004).

59. J. Habasaki, I. Okada and Y. Hiwatari, *Phys. Rev.* **B55**, 6309 (1997);

J. Habasaki and Y. Hiwatari, *Phys. Rev.* **E59**, 6962-66 (1999);

J. Habasaki and Y. Hiwatari, *Phys. Rev.* **E65**, 021604 (2002); J. Habasaki, *J. Non-Cryst, Solids,* **353**, 3956-3968 (2007).

60 Z. Hu and C. Margulis, Proc. Natl. Acad. Sci., USA, 103,831(2006).

61 J. Habasaki and K.L. Ngai, *J. Chem. Phys.,* 129,194501 (1-16) (2008).

62.W. Kob, C. Donati, S. J. Plimpton, P.H. Poole, S. C. Glotzer, Phys. Rev. Lett., 79, 2827(1997).

63. B. Doliwa and A. Heuer, J. Phys. Condens. Matt.,11, A277(1999).

64. F. Affouard, M. Descamps, L.-C. Valdes, J. Habasaki, P. Bordat and K. L. Ngai, *J. Chem. Phys,*131, 104510 (1-8) (2009).

65.A. Vegiri, J. Chem. Phys., 116 (2002).

66. P. R. Shorten and Tanya K Soboleva, Theoretical Biology and Medical Modelling **4, 18**(2007).

67. S. Sanyal, A. K. Sood, Prog. Theor. Phys. Suppl. 126, 163(1997).

68, E. R. Weeks, J. C. Crocker, A. C. Levitt, A. Schofield and D. A. Weitz, Science, 287, 28(2000).

69 J. Habasaki and Y. Hiwatari, *Phys. Rev.* **E65**, 021604 (2002).70. Tanaka and Araki, Phys. Rev. Lett., **85,** 1338(2000).

71. J. Depasse and A. Witillon, J. Colloid and Interface Sci., **33**, 430(1970).

72. D. J. Cole, M. C. Payne, G. Csányi, S. M. Spearing, and L. C. Ciacchi, J. Chem. Phys. **127**, 204704(2007).

73. A. A. Hassanali, S. J. Singer, *J. Phys. Chem. B*, 111, 11181(2007).

74. A. C. T. van Duin, A. Strachan, S. Stewman, Q. Zhang, X. Xu and W. A. Goddard, III, J. Phys. Chem., **107**, 3803(2003).

75. H. Manzano, S. Moeini, F. Marinelli, A. C. T. van Duin, F-J Ulm and R. J.-M Pellenq, J. Am. Chem. Soc., **134**, 2208(2012).

76. G. K. Lockwood and S. H. Garofalini, Chem. Phys., 131, 074703(2009).

77. J. C. Fogarty, H. M. Aktulga, A. Y. Grama, A. C. T. van Duin and A. A. Pandit, J. Chem. Phys., **132**, 174704(2010).

78. R. Tuinier, J. Rieger , C. G. de Kruif, Adv. Colloid and Interface Science, **103**,1(2003).

79. T. Araki and H. Tanaka, *J. Phys.:Condens. Matter ,* **20**, 072101(2008).

80. A. A. Milischuk and B. M. Ladanyi, J. Chem. Phys.,**135,** 174709(2011).

81. A. K. Rappé and W. A. Goddard III, J. Phys. Chem., **95**, 3358(1991).

82. E. Demiralp,T. C¸ ag˘in, and W. A. Goddard III , Phys. Rev. Lett., **82**, 1708(1999).

83. Y. Ida, Phys. Earth Planet, Interiors, **13,** 97(1976).

84. J. Habasaki and I. Okada, Molecular Simulation, **9**, 319(1992).

85. V. A. Bakaev and W. A. Steele, J. Chem. Phys., **111**, 9803(1999).

86. R. T. Cygan, J-J Liang, and A. G. Kalinichev, J. Phys. Chem. B, **108**, 1255 (2004).

87. I. S. Joung and T. E. Cheatham, III, J. Phys. Chem. B, **112**, 9020(2008).

Figure captions

Fig. 1 (a) Structure of colloidal units represented using a ball-and-stick model. (b) Polyhedral structure composed of SiO_4 units.

Fig. 2 Structure of system (a) I-A and (b) I-B.

The Si positions are emphasised by large yellow spheres. Blue: Na, Pale blue: Cl, White: H, Red: O.

Fig. 3 (a) Network of system II-A projected onto the xy plane. This system does not contain NaCl. Si atoms are represented by blue spheres, and O atoms are represented by red spheres. The Si-O bonds are also indicated. Some colloidal units tend to connect to form larger clusters that consist of several units. These clusters are separated by water but form fractal structures that incorporate water. Nineteen clusters are evident in the 3D view of the unit cell under rotation (not shown), but the entire colloidal system appears to be connected when it is projected onto a 2D plane. (b) Network of system II-A depicted in black and white and used for the fractal-dimension analysis of the 2D projection (see Table 2). The values for the medium-length-scale region were obtained using boxes with side lengths shorter than the red (shorter) line, whereas those for the longer-scale region were obtained using boxes with side lengths between those of the red (shorter) and blue (longer) lines in the figure.

Fig. 4 Network of system II-C : (a) a projection onto the plane and (b) the 3D structure of the unit cell. The aggregation is developed.

Fig. 5 Network structure of system I-C (gel) projected onto each of three perpendicular planes. Water and Na and Cl ions are omitted for clarification. The system exhibits a 3D percolation of aggregates. This situation can be referred to as “super-aggregation”.

Fig. 6 (a) Pair correlation functions of Si-Si pairs in systems I-A (pink, dotted curve), I-C (red, dot dashed curve), II-A(black, dotted curve) and II-C (blue, solid curve) on a log-linear plot and (b) the same functions on a log-log scale. A power-law region and a region

corresponding to g(r)~1 with some deviations are observed. The g(r) function displays a clear minimum (corresponding to the barrier in the potential of mean force) near r=30 (Å) in the system without salt, in which the clusters are isolated. (c) Running coordination functions of Si-Si pairs on a log-log plot. The fitted lines represent fits to the power-law regions (typically 4~20 Å). The slopes for the longer regions characterise the super-aggregation of the aggregates.

Fig. 7 (a) Comparison of pair correlation functions, g(r), in the power-law region for systems I-C (solid curves) and II-A (dashed curves). Black: Si-Si, Red: Si-O, Blue: Si-OW, Pink: Si-HW, Green: Si-Na^+, Brown: Si-Cl^-. In II-A, the contribution of the SiO_2 component decreases with increasing *r*, while that of the water component gradually increases. In I-C, the slopes of these components flatten, indicating the mixing of these structures. (b) Running coordination numbers for System II-A. (c) Running coordination numbers for System I-C. The colours in (b) and (c) are the same as in (a). The functions for the Si-Si and Si-O pairs are the counterparts of the functions for the water components (Si-OW and Si-HW), which are affected by the salt concentration.

Fig. 8 Pair correlation functions of water for systems (a) I-A, (b) I-B and (c) I-C after gelation.
Purple: OW-OW pairs, Blue: HW-HW pairs, Red: OW-HW pairs. With the addition of salt, the first peak in the g(r) for the OW-OW pair splits, and this splitting becomes clearer in the gel. A long-range structure indicated by waves in the longer-*r* region also appears. Some small changes are also observed for the other pairs. These changes are similar to those associated with the LDL-to-HDL transition in water (see text).

Fig. 9 (a) MSD of each species in system I-A. (b) MSD of each species in system I-B.
(c) MSD of each species in system I-C. With the formation of infinitive networks, the motions of all species tend to plateau. This phenomenon is considered to signify the formation of a gel.

Fig. 10 Heterogeneous dynamics found in system I-C. Squared displacements of arbitrary chosen four oxygen atoms in silica part and those in water (upper panel). Mobile atoms are for water. Squared displacements of arbitrary chosen eight atoms in silica part (lower panel).

(a)

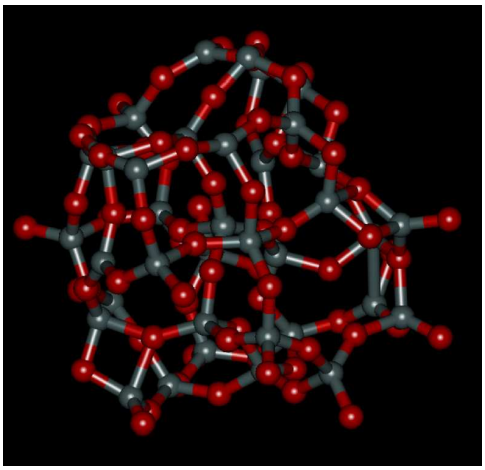

(b)

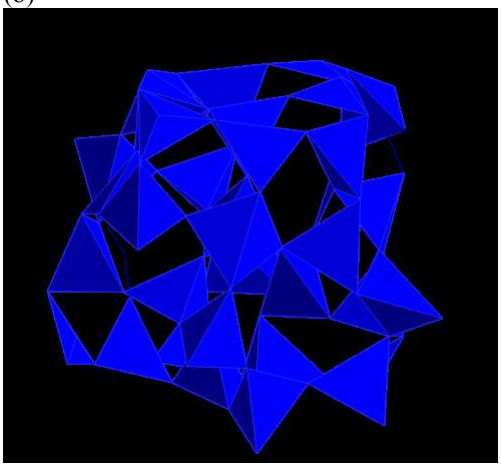

Fig. 1

(a)

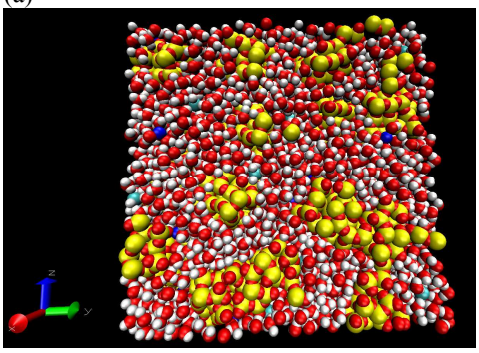

(b)

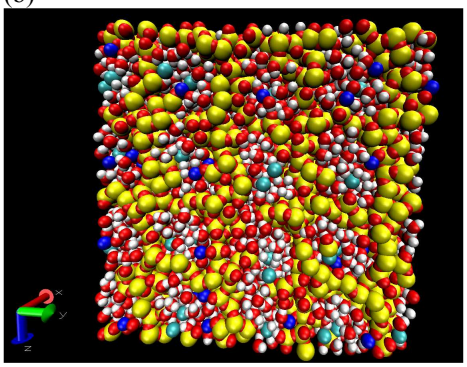

Fig. 2

(a)

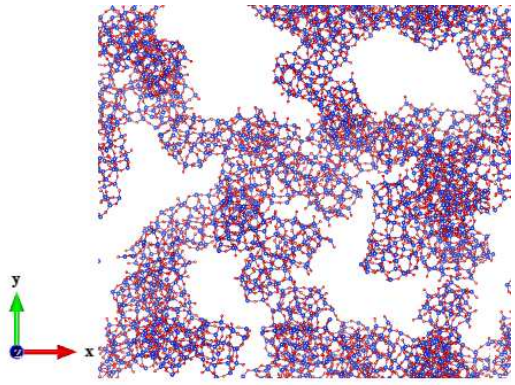

(b)

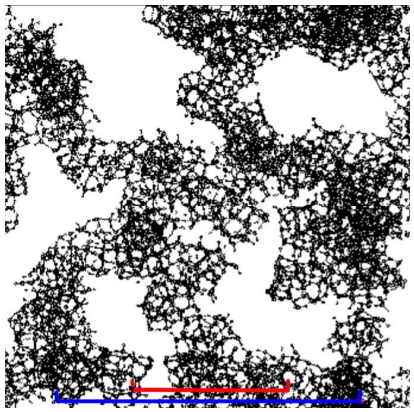

Fig. 3

(a)

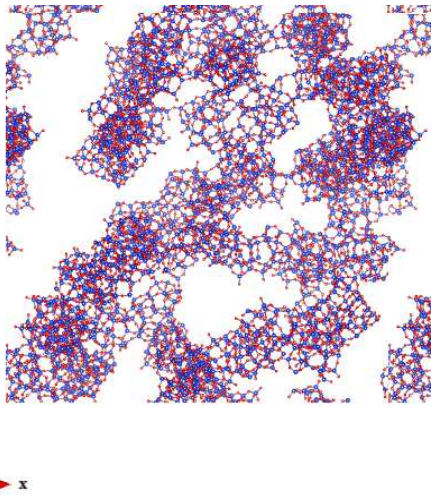

(b)

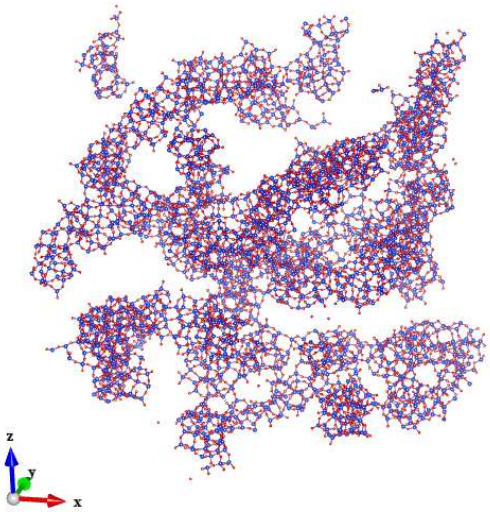

Fig. 4

(a)

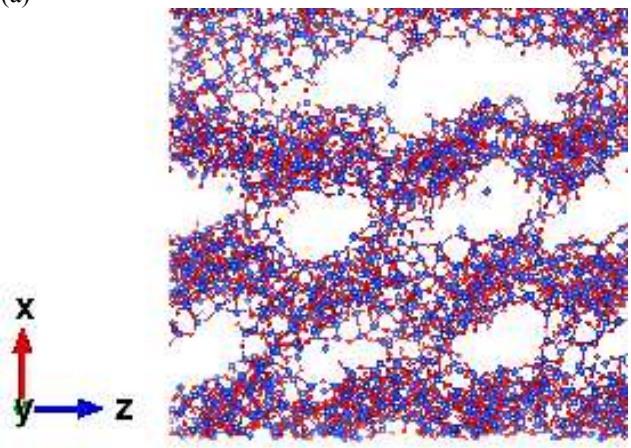

(b)

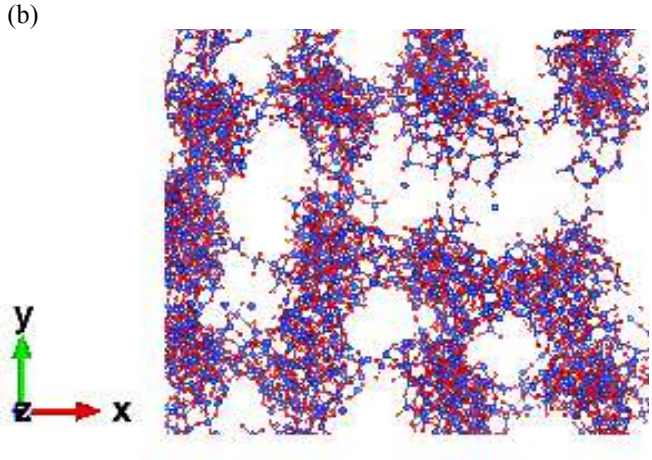

(c)

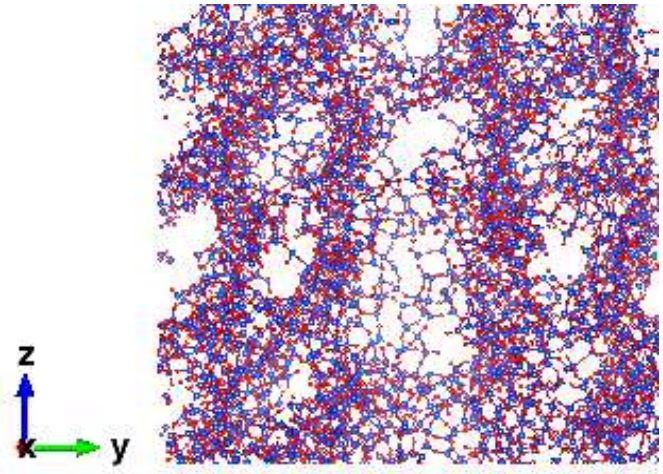

Fig. 5

(a)

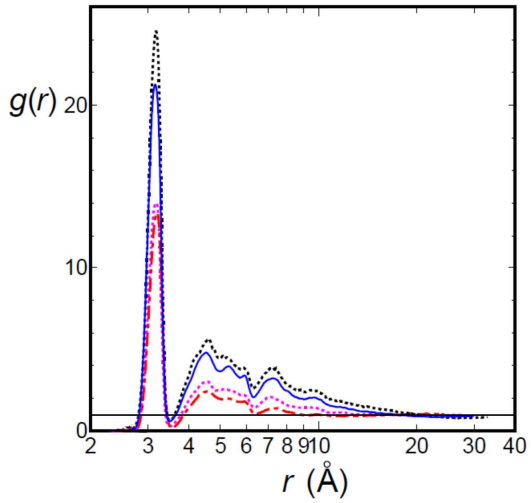
g(r)
20
10
0
2 3 4 5 6 7 8 9 10 20 30 40
r (Å)

(b)

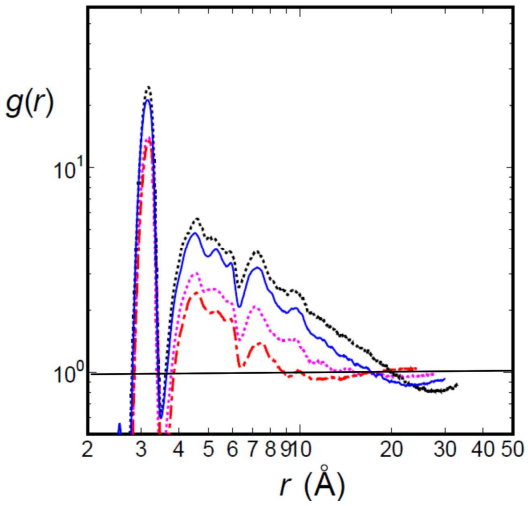
g(r)
10^1
10^0
2 3 4 5 6 7 8 9 10 20 30 40 50
r (Å)

(c)

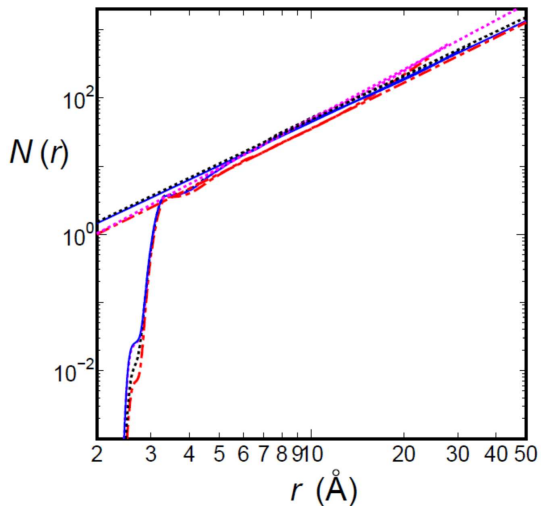
10^2
N (r)
10^0
10^-2
2 3 4 5 6 7 8 9 10 20 30 40 50
r (Å)

Fig. 6

(a)

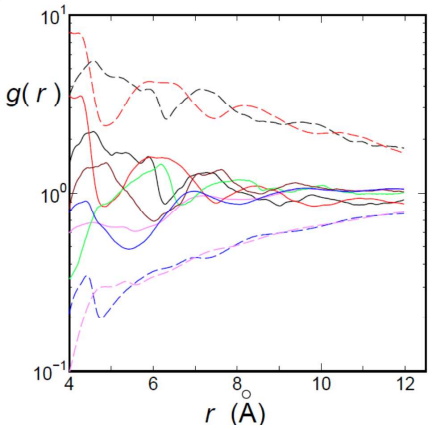
10^1
$g(r)$
10^0
10^{-1}
4
6
8
10
12
r (Å)

(b)

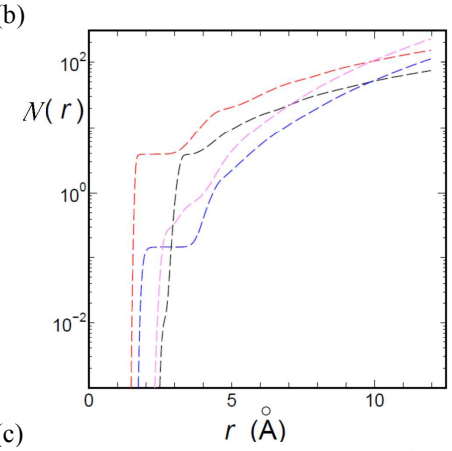
10^2
$N(r)$
10^0
10^{-2}
0
5
10
r (Å)

(c)

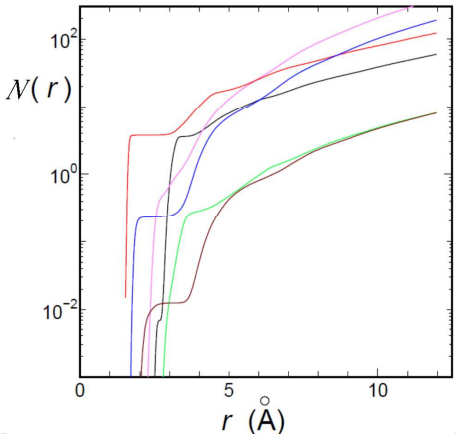
10^2
$N(r)$
10^0
10^{-2}
0
5
10
r (Å)

Fig. 7

(a)

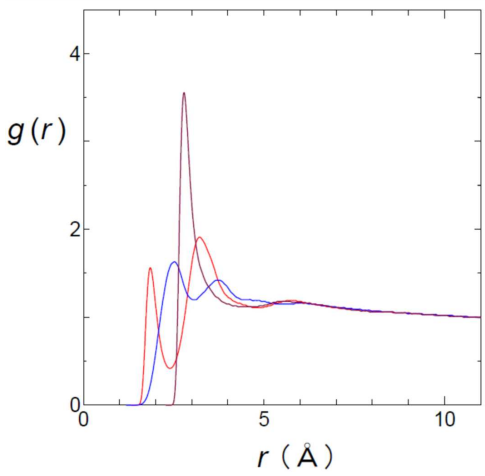

(b)

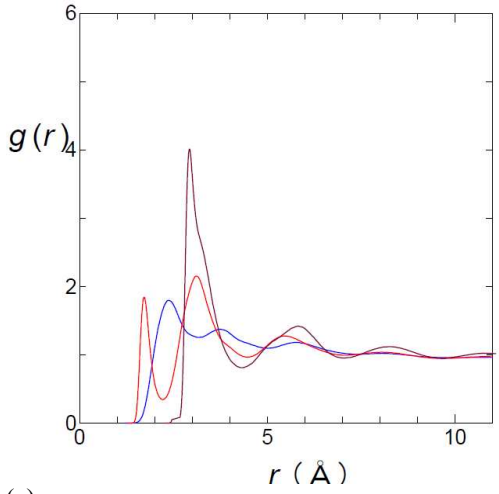

(c)

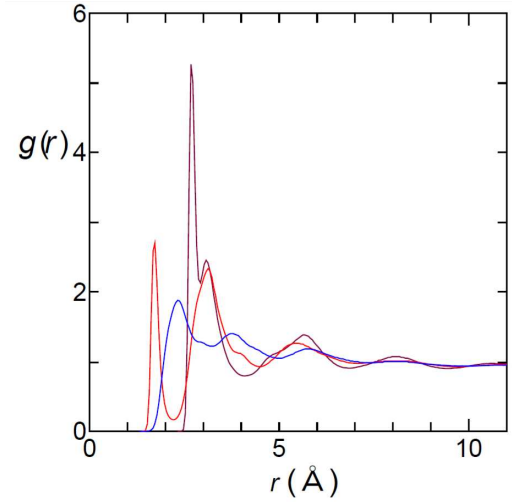

Fig. 8

(a)

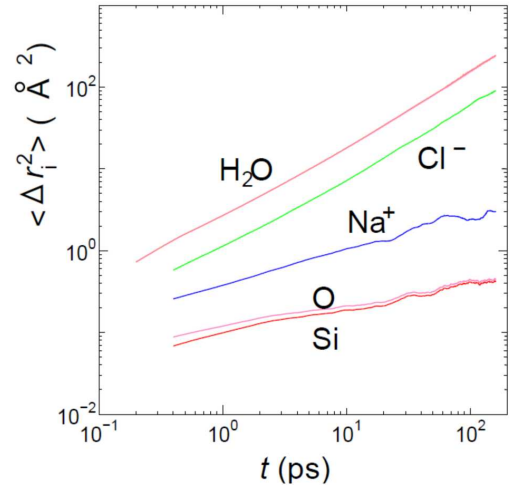
$<\Delta r_i^2>$ (Å^2)
10^2
10^0
10^{-2}
10^{-1}
10^0
10^1
10^2
t (ps)
H_2O
Cl^-
Na^+
O
Si

(b)

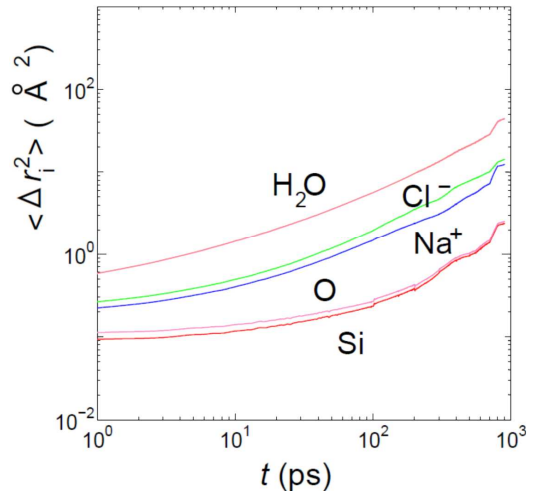
$<\Delta r_i^2>$ (Å^2)
10^2
10^0
10^{-2}
10^0
10^1
10^2
10^3
t (ps)
H_2O
Cl^-
Na^+
O
Si

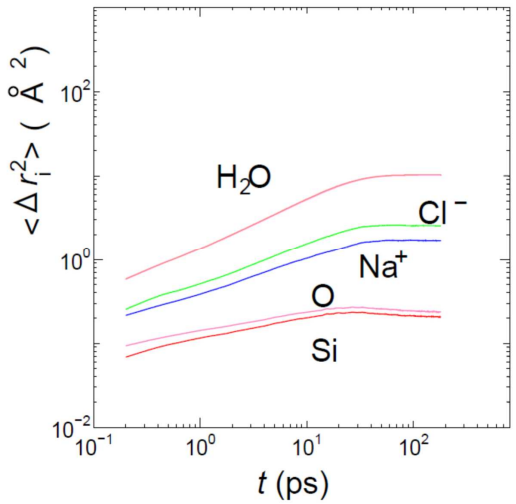
$<\Delta r_i^2>$ (Å^2)
10^2
10^0
10^{-2}
10^{-1}
10^0
10^1
10^2
t (ps)
H_2O
Cl^-
Na^+
O
Si

Fig. 9

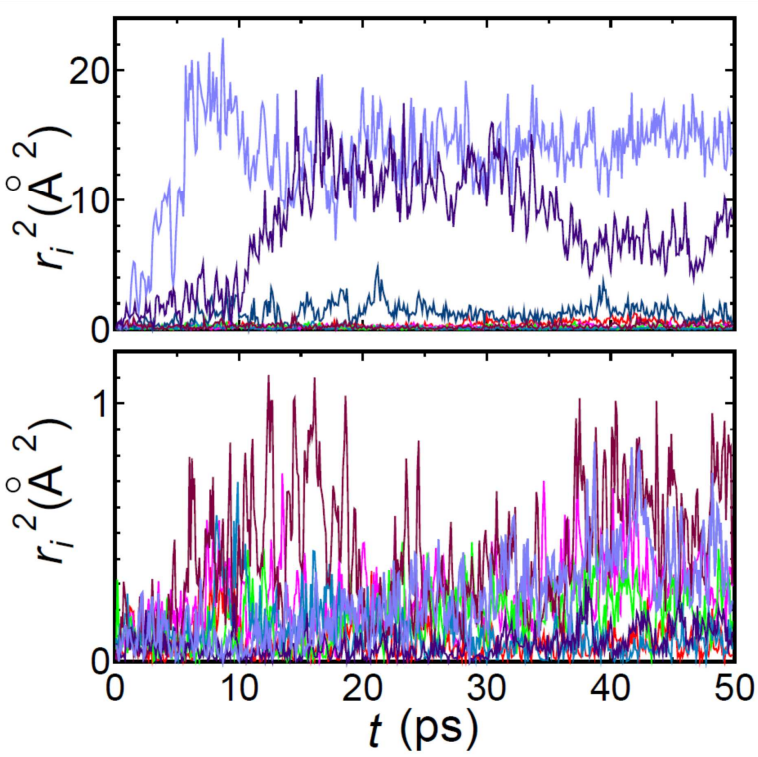

Fig. 10